Journal of Electronic Materials (2024) 53:5212–5221
https://doi.org/10.1007/s11664-024-11228-0

28TH INTERNATIONAL CONFERENCE ON NUCLEAR TRACKS AND RADIATION MEASUREMENTS

Dispersion-Engineered SiN-Coated TeO_2 Hybrid Waveguide for Nonlinear Applications

Kanika[1] · Neena Jaggi[1] · Than Singh Saini[1]

Received: 6 February 2024 / Accepted: 30 May 2024 / Published online: 18 June 2024

Abstract
On-chip light generation in the mid-infrared (mid-IR) region of the electromagnetic spectrum is gaining considerable attention due to its various potential applications in free-space communication, mid-IR spectroscopy, sensing, and thermal Imaging. In this work, we have designed a dispersion-engineered silicon nitride (SiN)-coated tellurium oxide (TeO_2) hybrid waveguide on silica (SiO_2) substrate with barium fluoride (BaF_2) as cladding for nonlinear applications. Strong modal confinement, broad dispersion characteristic, and high nonlinearity were achieved in the proposed hybrid waveguide design, which are important features for obtaining desired nonlinear applications. Through numerical simulations, we found that the dispersion curve is nearly flat within the dispersion range of −40.60 ps/nm/km to 33.15 ps/nm/km for a spectral bandwidth of 1.55–4.25 µm with a zero-dispersion wavelength (ZDW) around 1.80 µm, which is suitable for generating nonlinear effects such as four-wave mixing, self-phase modulation, and Raman scattering. Such types of on-chip hybrid waveguide devices can be pumped using a commercially available fiber laser operating at a wavelength of 2 µm. The design of the hybrid waveguide was optimized to achieve very low modal confinement loss ranging from 0.1×10^{-4} to 35 dB/cm, with a spectral bandwidth of 1.5–4 µm. Additionally, a high nonlinear coefficient value of 1372 W^{-1} km^{-1} was achieved at a pumping wavelength of 1.5 µm in hybrid waveguide. The results of such hybrid waveguides can be helpful to experimentalists working in this field for developing nonlinear hybrid waveguide devices. These nonlinear hybrid waveguide devices have potential nonlinear applications, including four-wave mixing, Raman scattering, and supercontinuum spectrum spanning the near-IR to mid-IR. Further, the on-chip hybrid waveguide structure can be significantly help to expand the functionality of future photonics integrated circuits.

Keywords Hybrid waveguide · dispersion · zero-dispersion wavelength · Nonlinearity

Introduction

In recent years, there has been an emphasis on understanding the physics underlying the intricate subject of nonlinear optical physics (intensity-dependent optical properties of material).[1] Some of the nonlinear phenomena are self-phase modulation (SPM), cross-phase modulation (XPM), stimulated Raman scattering (SRS), four-wave mixing (FWM), and many others.[2] SPM generates new frequency components and broadens the spectrum due to phase modulation caused by changes in light intensity in the pulse itself.[2,3] SRS is a process of interaction between incident photons and molecular vibrations, causing them to generate new frequency components towards the lower-frequency domain.[2,4] FWM generates new frequencies on the lower side and the higher side of the input pulse spectrum under phase matching conditions.[2,5] There are various noteworthy uses of nonlinear optical phenomena across many domains, such as frequency conversion, optical parametric oscillators (OPO), optical switching and modulation, nonlinear optical microscopy, quantum nonlinear optics, and supercontinuum generation, which have fascinated many researchers in this field.[1,2] One of the astonishing nonlinear phenomena is supercontinuum (SC) generation (the ultra-broadening of a short intense laser pulse after passing through a highly nonlinear media),[6] which has become an intense focus of

✉ Than Singh Saini
tsinghdph@gmail.com

[1] Department of Physics, National Institute of Technology Kurukshetra, Kurukshetra 136119, HR, India

research because of its various dramatic applications such as broadband laser sources, gas sensing, military purposes, and various clinical analyses such as optical coherence tomography and other areas.[6–9] SC spectra are coherent laser sources generated through nonlinear processes such as SPM, FWM, SRS, and dispersion characteristics of a nonlinear material.

To achieve stable, smooth, un-depletable, coherent, and wide SC spectra, the pumping wavelength of the input fiber laser source is around a zero-dispersion wavelength (ZDW) of nonlinear material, and this material should have a flat and low dispersion profile that falls in the anomalous dispersion region.[6,7] A wide range of advantages can be obtained from the generation of SC spectra in the anomalous dispersion region, including the production of extremely broadband spectra that span from the visible to the near-infrared or even mid-infrared regions. SC spectra can also be tuned by varying parameters like pump power, pulse duration, and the properties of the nonlinear medium, and they offer high optical power density across broad spectra. However, the pumping in the anomalous dispersion regime, the broadening mechanism of the SC spectrum, is due to the modulation instability or soliton fission on the anomalous side of the dispersion profile together with the emission of dispersive waves in the normal dispersion region. The SC spectrum generated by the soliton dynamics is susceptible to the laser shot noise, and the output pulse shows a complex temporal structure which makes recompression difficult.[6,10] The generation of on-chip light sources in the mid-infrared (mid-IR) region spanning wavelengths from 2 μm to 25 μm has attracted considerable research attention due to its fascinating applications in fluorescence microscopy, imaging,[11] and free space communication,[12] as a transparency window of earth atmosphere lies between 2 μm and 5 μm and 8–13 μm. This region is also known as the molecular fingerprinting region because it contains most of the vibrational transitions that occur in molecules. These features can be used in various fields such as medicine and security.[7,13,14] Most previous numerical and experimental studies for the generation of mid-IR light sources were conducted using silica (SiO_2), bismuth, chalcogenide, and tellurite fibers, integrated waveguides, or photonic crystal fibers (PCF).[15–19] Silica PCF geometry has high modal confinement but it has weak nonlinearity, and a high-power pumping source is required; also, its transparency is below 2.4 μm, so it cannot be used for mid-IR light generation. Chalcogenide, tellurite, and fluoride materials have high nonlinearity, and their transparency lies in the mid-IR region. However, the ZDW of these highly nonlinear materials lies in the mid-IR region, and there is a lack of available fiber laser sources operating at these large wavelengths. High nonlinearity and pumping around the ZDW reduce the power requirement of the input laser source. Researchers are looking for new designs and ways to modify the properties of materials to achieve the desired ZDW of nonlinear material, and to obtain flat and wide dispersion characteristics to produce broad, stable, non-depletable light sources in the mid-IR domain.[20–27]

During the previous decade, Choi et al. showed that Ge–Sb–S chalcogenide glasses were the subject of much research due to their nonlinear optical characteristics. It was demonstrated that with its huge refractive index and wide transparency range, this waveguide has a nonlinear parameter of 7 W^{-1}/m at 1.5 μm and generates SC spectra between 1280 nm and 2120 nm, which makes this ridge waveguide a promising platform for future nonlinear applications in the infrared domain.[28] Saini et al. designed and numerically analyzed an on-chip rib Ga–Sb–S chalcogenide waveguide structure for mid-IR SC generation. Numerical investigations showed that the waveguide has two ZDWs at 2050 nm and 2800 nm with nonlinear coefficients of 24,100 W^{-1} km^{-1} and 14,000 W^{-1} km^{-1}, respectively. When driven by 97-fs laser pulses with a peak strength of 1 kW at 2050 nm, the waveguide structure produces a mid-IR SC spectrum ranging from 1000 nm to 7800 nm.[29] Further, SC spectra ranging from 1.2 μm to 7.2 μm are generated in an As_2Se_3 chalcogenide glass on-chip rib waveguide structure when pumped with an input laser pulse of 200 fs at 2.8-nm wavelength with peak power of 2.5 kW.[30] Medjouri et al. numerically investigated an As_2S_5 chalcogenide glass ridge waveguide structure. This waveguide structure exhibits a ZDW around 2 μm and generates ultra-broad, flat, stable SC spectra spanning from 700 nm to 5200 nm driven by 25 kW power 100-fs laser source operating at a wavelength of 2050 nm. It has been used for sensing, military purposes, and other applications.[31] Sinobad et al. reported a highly coherent octave-spanning mid-IR on-chip broad laser source in an air-clad Si–Ge/Si waveguide.[32] Terro et. al. reported a low-loss germanium-on-silicon photonic integrated device generating a broad bandwidth mid-IR spectra of 3.39–6.02 μm at a pumping wavelength of 4.6 μm using a 200-fs optical parametric amplifier (OPA) laser source.[33] Gyger et al. investigated simulated Brillouin zone scattering for the first time in silicon nitride (SiN) completely coated with silica cladding.[34] Furthermore, Saini and Supradeepa reported the design and analysis of a tellurium oxide (TeO_2)-coated SiN hybrid waveguide on a sapphire substrate that extends SC spectra from 0.88 μm to 5.22 μm or 0.95 μm to 5.50 μm at pumping wavelengths of 1.55 μm and 2 μm, respectively, using a pump peak power of 10 kW. By using sapphire as substrate instead of silica, the transparency window increases up to 7 μm.[35] Zhang et al. numerically studied single-layer double-core Si_3N_4 coupled waveguides having four ZDWs. This on-chip waveguide design generated a 750–3001-nm broad spectrum using an input hyperbolic secant pulse of 50 fs, in the anomalous region.[36] Sheikhmolaee et al. proposed a GAP-Se tapered

hybrid chalcogenide planner rib waveguide that has two ZDWs at 2.81 µm and 4.91 µm for nonlinear application.[37] Botter et al., for the first time, observed a stimulated Brillouin scattering third-order nonlinear effect in a TeO_2 -coated SiN waveguide.[38] Mbonde et al. recently reported that complementary metal–oxide–semiconductor (CMOS)-compatible thin Si_3N_4 coated with TeO_2 on SiO_2 substrate enhances nonlinearity 2.5 times, making the perfect element for nonlinear applications on integrated photonics devices.[39]

Furthermore, TeO_2 is a highly promising oxide glass that has high linear and nonlinear optical properties. It can be investigated as optical fibers, integrated photonics circuits for four-wave mixing, broadband Raman amplification, rare-earth-metal-doped amplifiers, laser sources, and SC generation.[39–42] It has a high-value linear and nonlinear refractive index, 20 times more than silica fiber.[35] It has transparency in visible to mid-IR regions with low loss and low dispersion value with a high Raman gain coefficient.[43–45] CMOS-compatible SiN is transparent in the visible to infrared domain.[46,47] Its high performance, transparency, compactness, low loss, and cost-effectiveness make it perfect for photonic integrated devices, and it has various applications in gas sensing, clinical investigation, amplifiers, and laser sources.[48,49] Like TeO_2, SiN also has a high linear and nonlinear refractive index, providing a good platform for nonlinear optical properties. Considering BaF_2 as the upper layer rather than considering no cover layer has provided advantages. BaF_2 is a versatile optical window material with low dispersion and a broad transparency range from the ultraviolet to the far-infrared.[50,51] Using BaF_2 as covering in comparison to no covering layer or air as the covering layer results in a low dispersion value. A low dispersion profile is crucial for maximizing SC generation in fibers by reducing temporal walk-off during spectral broadening. Also, there is little variation in confinement loss using BaF_2 in the spectral range of 1.5–4 µm.

Recently, a high-quality TeO_2 waveguide integrated on a low-loss SiN wafer-scale platform was fabricated for the application of compact linear, nonlinear, and active devices operating in visible to mid-IR regions.[44] However, through numerical simulations, we found a deep-normal (deep-negative) dispersion profile of the fabricated TeO_2 integrated waveguide on the SiN platform.[44] Also, another TeO_2-coated SiN hybrid waveguide was reported for near- to mid-IR SC generation.[35] This hybrid waveguide also has a dispersion profile in the normal dispersion region, and the ZDW lies around 3.5 µm, which is not suitable for nonlinear applications such as four-wave mixing and SC spectrum generation using conventional laser pumping at 1.55 µm and 2.0 µm.

In this work, we have designed and analyzed a dispersion-engineered SiN-coated TeO_2 hybrid waveguide on SiO_2 substrate with BaF_2 as cladding for nonlinear applications. Dispersion characteristics, modal confinement loss, and nonlinearity are important features to achieve the desired results. By simulating this hybrid waveguide design, we have obtained a broad and low-value dispersion curve lying in the anomalous region, low confinement loss, and high nonlinearity for the wavelength spanning from 1.55 µm to 4.25 µm. The designed hybrid waveguide structure is highly applicable for future on-chip photonic integrated circuits. A designed hybrid SiN-coated TeO_2 waveguide device can be a significant choice to expand its functionality towards nonlinear applications using commercially available laser pulses operating at 2 µm.

Design and Proposed Fabrication Method for the Hybrid Waveguide Structure

The schematic transverse cross-sectional view of the designed SiN-coated TeO_2 hybrid waveguide on silica substrate with BaF_2 as cladding is illustrated in Fig. 1, where w is the width of the TeO_2 strip, h_1 represents the thickness of the TeO_2 strip, and h_2 indicates the thickness of the SiN layer coated over the TeO_2 strip. Seventy percent of the thickness of the SiN layer is considered on both sides of the TeO_2 strip. From a fabrication point of view, the TeO_2 film can be deposited on a 2-µm-thick SiO_2 substrate. This type of waveguide structure can be obtained by employing radio-frequency (RF) reactive sputtering or liquid-phase chemical vapor deposition (LPCVD) techniques.[35] Following the RF sputtering technique, coating of SiN layer over TeO_2 strip can be obtained. The pattern of a hybrid waveguide device can be fabricated using electron beam lithography and reactive ion etching (RIE) techniques.[43] Additionally, a 2-µm-thick cladding layer of BaF_2 is deposited using the spin-coating method. Finally, a hybrid waveguide structure is obtained. The optimized geometrical parameters of hybrid waveguide are illustrated in Table I. The core region of the designed hybrid waveguide shows several modes. To avoid inter-modal coupling between these modes, mode-coupling

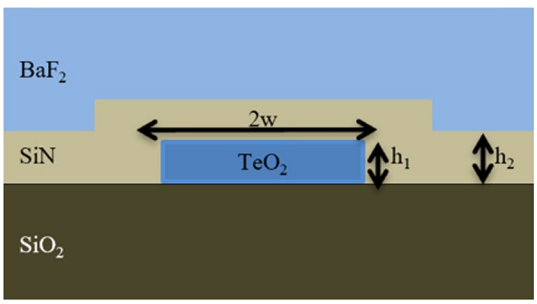

Fig. 1 A transverse cross-sectional view of a SiN-coated TeO_2 hybrid waveguide.

suppression conditions are satisfied by the effective indices of the modes.[52] Only the fundamental transverse electric (TE) mode is considered during the whole numerical simulation, since higher-order modes have larger confinement losses. Figure 2a–d shows the distribution of electric fields for confined fundamental TE modes at pumping wavelengths of 1.5 µm, 2 µm, 3 µm, and 5 µm.

Table I Optimized geometrical parameters of the hybrid waveguide design

Parameters	Value
h_1 (thickness of TeO_2 layer)	470 nm
h_2 (thickness of SiN strip)	580 nm
w (width of TeO_2 layer)	3 µm

Numerical Method Analysis

To explore the design of a SiN-coated TeO_2 hybrid waveguide, the TE modes passing through this hybrid waveguide were simulated and their effective mode indices were calculated using the full-vectorial finite element method (FEM). COMSOL Multiphysics (an adaptable simulation tool) supports FEM for solving problems in the previously mentioned investigations. With the variation in the wavelength of the input laser pulse, changes in the refractive index of the material are observed. This variation in the refractive index of TeO_2, SiN, SiO_2, and BaF_2 materials is calculated using the Sellmeier equation (Eq. 1) and Sellmeier coefficients of these materials as shown in Table II.[35]

$$n^2 = A_0 + \sum_{n=1}^{n} \frac{A_n \lambda^2}{\lambda^2 - a_n^2} \tag{1}$$

Understanding and controlling nonlinear optical properties is greatly aided by group velocity dispersion (GVD), especially when it comes to optical fibers and other

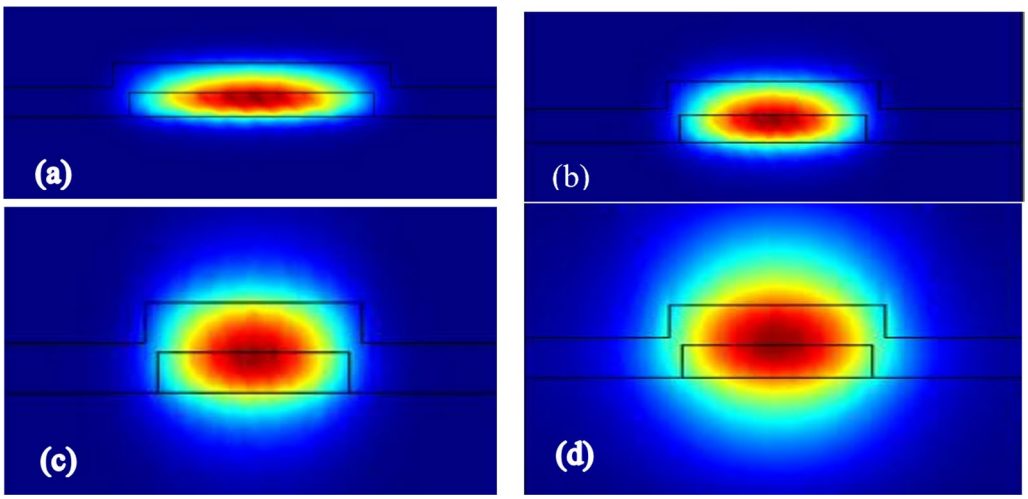

Fig. 2 Electrical field distribution of fundamental TE modes confined in the core region of the hybrid waveguide at pumping wavelengths of (a) 1.55 µm, (b) 2 µm, (c) 3 µm, and (d) 5 µm.

Table II Sellmeier coefficients for TeO_2, SiN, BaF_2, and SiO_2[35,51]

Sellmeier coefficient	TeO_2 (λ in µm)	SiN (λ in nm)	BaF_2 (λ in µm)	SiO_2 (λ in µm)
A_0	3.5483034	1	1.3397	1
A_1	0.9783726	3.0249	0.8107	0.6961663
A_2	6.6510879	40314	0.19652	0.4079426
A_3	–	–	4.52469	0.8974794
a_1	0.287522973	135.3406	0.10065	0.0684043
a_2	15	1239842	29.87	0.1162414
a_3	–	–	53.82	9.896161

waveguides. Various components of input laser pulses may disperse over time as they pass through the fibers due to GVD, leading to pulse broadening. High-intensity light can induce new frequency components. Differences in group velocity of these new frequency components can affect the features and effectiveness of nonlinear processes. In the anomalous dispersion domain, nonlinear phenomena may occasionally counteract GVD and solitons may develop. For optimization of optical nonlinear systems, dispersion needs to be considered, and the dispersion profile of the hybrid waveguide can be simulated using Eq. 2.[35]

$$D = -\frac{\lambda}{C}\frac{\partial^2 \mathrm{Re}\left(n_{e_{FF}}\right)}{\partial \lambda^2} \tag{2}$$

where c represents the speed of light, and $\mathrm{Re}(n_{eff})$ is the real part of the effective mode indices. The effective area of a mode traveling through a hybrid waveguide and its nonlinear coefficient is given by Eqs. 3 and 4, respectively.[35]

$$A\mathrm{eff} = \frac{\left(\int_{-\infty}^{\infty}\int |\mathrm{E}|^2 dxdy\right)^2}{\left(\int_{-\infty}^{\infty}\int |\mathrm{E}|^4 dxdy\right)} \tag{3}$$

$$\gamma = \frac{2\pi n_2}{\lambda A_{e_{FF}}} \tag{4}$$

where E denotes the amplitude of the electric field intensity, n_2 is the nonlinear refractive index for TeO_2, and $n_2 = 1.3 \times 10^{-18}$ m^2/W.[35] We consider only the TeO_2 nonlinear refractive index when calculating the effective nonlinearity because at shorter wavelengths of 1.55 µm and 2 µm, most of the light of the fundamental mode is confined in the TeO_2 core region rather than in the SiN strip region. Light starts to be confined in a SiN strip at higher wavelengths, as shown in Fig. 2. Also, confinement loss is very large beyond 4.5 µm. This hybrid waveguide can be advantageous for nonlinear applications within the wavelength range up to 4.5 µm.

Result and Discussion

Dispersion and nonlinearity play a major role in understanding and managing nonlinear optical characteristics of photonic-integrated devices. Proper dispersion engineering allows us to employ conventional laser sources for the characterization of such devices. We have designed our hybrid waveguide structure for obtaining its ZDW near 2 m. The dispersion characteristics of a reported hybrid waveguide are shown in Figs. 3, 4, 5, and 6.

Figure 3 shows the change in dispersion characteristics with a change in thickness (h_1) of the TeO_2 strip at $h_2 = 580$ nm and $w = 3$ µm. It can be seen that with an increase in the thickness of TeO_2 strip, the dispersion curve shifts from a normal dispersion domain to an anomalous dispersion domain, and the value of the ZDW shifts towards the lower-wavelength region. Further, the dispersion curve becomes progressively flatter on increasing h_1.

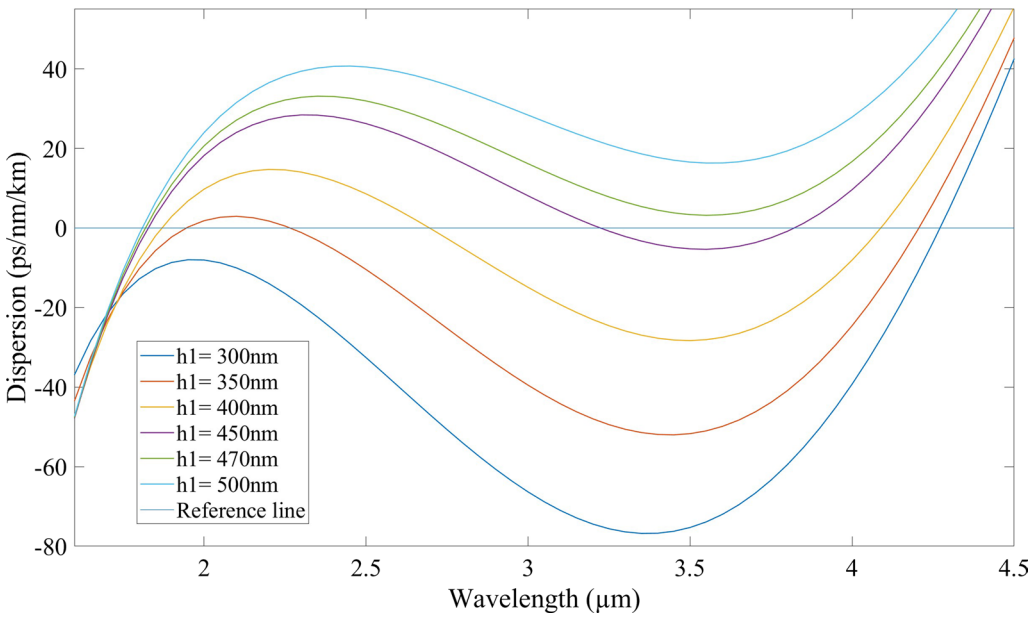

Fig. 3 Dispersion profiles of a SiN-coated TeO_2 hybrid waveguide with variation in thickness (h_1) of the TeO_2 core at $w = 3$ µm and $h_2 = 580$ nm.

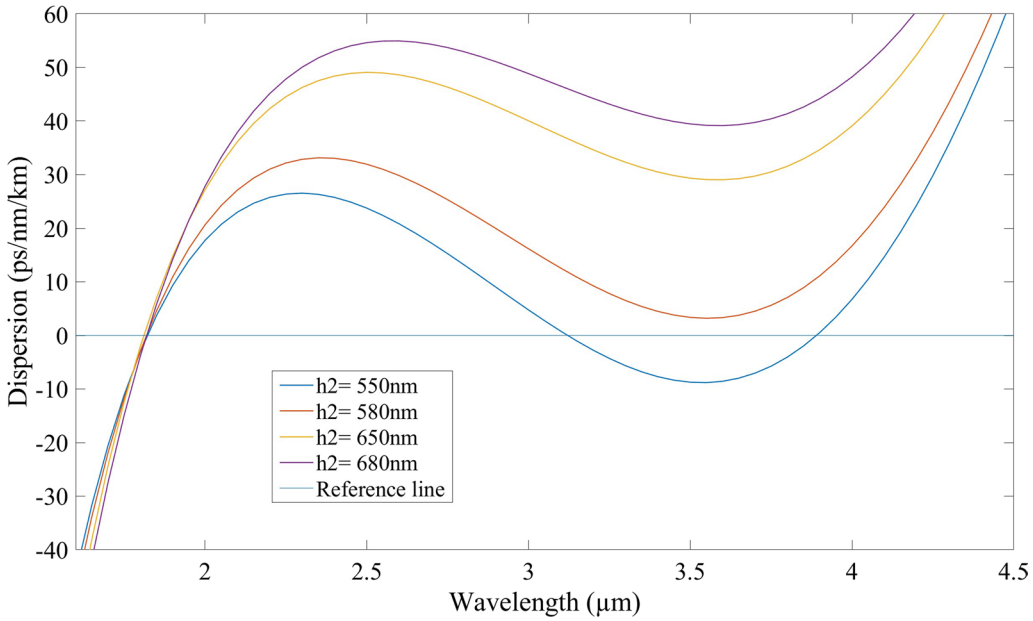

Fig. 4 Dispersion profiles of a SiN-coated TeO_2 hybrid waveguide with variation in thickness (h_2) of SiN at $h_1 = 470$ nm and $w = 3$ μm.

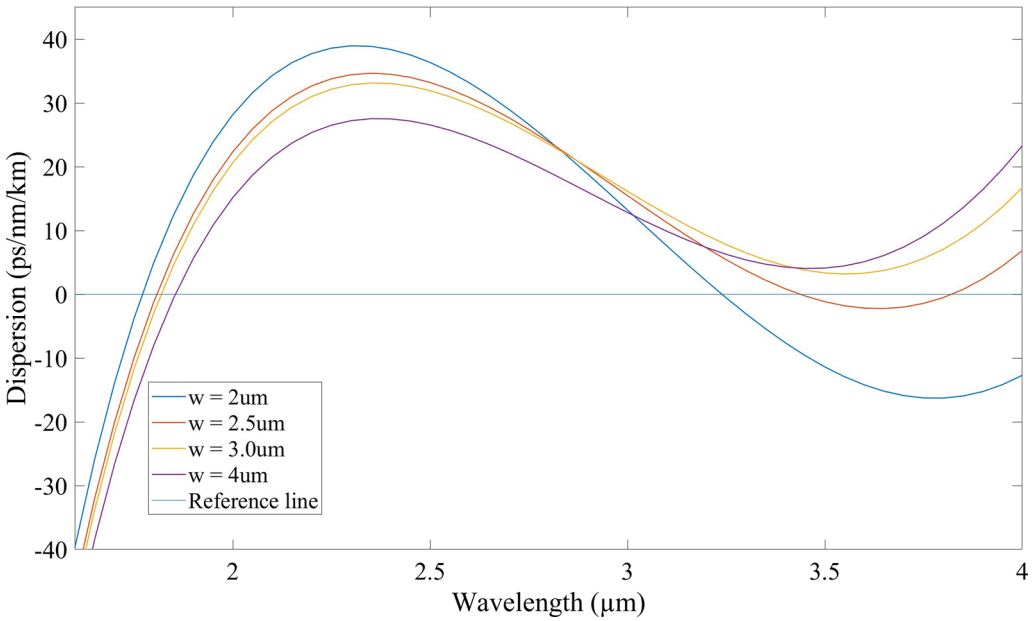

Fig. 5 Dispersion profiles of a SiN-coated TeO_2 hybrid waveguide with variation in the width (w) of TeO_2 at $h_1 = 470$ nm and $h_2 = 580$ nm.

Figure 4 presents the variation in dispersion characteristics with an increase in thickness (h_2) of coated SiN layer at $h_1 = 470$ nm and $w = 3$ μm. It can be observed that with an increase in the thickness of the SiN layer, the dispersion curve shifts towards a higher dispersion value.

Figure 5 presents the change in dispersion characteristics with an increase in the width (w) of the TeO_2 strip at $h_1 = 470$ nm and $h_2 = 580$ nm. It is observed that the dispersion curve shifts to a lower dispersion value and the ZDW shifts towards a higher wavelength with an increase in the width of the TeO_2 strip. Modal dispersion and a ZDW in a waveguide are affected by the thickness and width of the core due to its effect on the mode distribution, effective refractive index, and mode confinement. Thicker cores provide optical modes more room to spread out in the transverse direction. This is why it is expected that as the thickness of the core increases, there is an increase in the dispersion

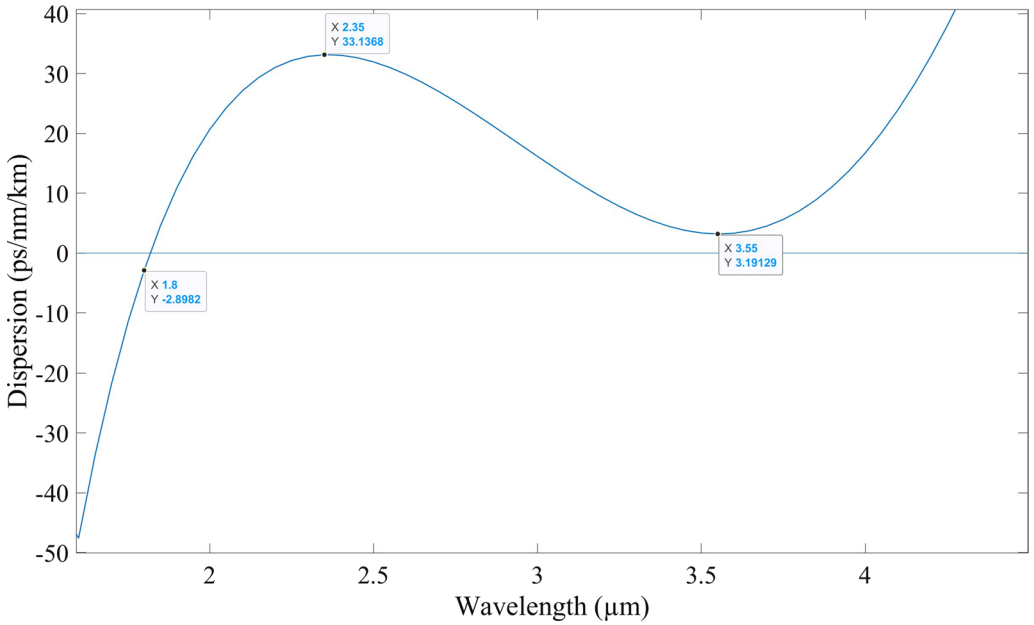

Fig. 6 Dispersion profile of the proposed hybrid waveguide structure with optimized geometrical parameters $h_1 = 470$ nm, $h_2 = 580$ nm, and $w = 3$ μm.

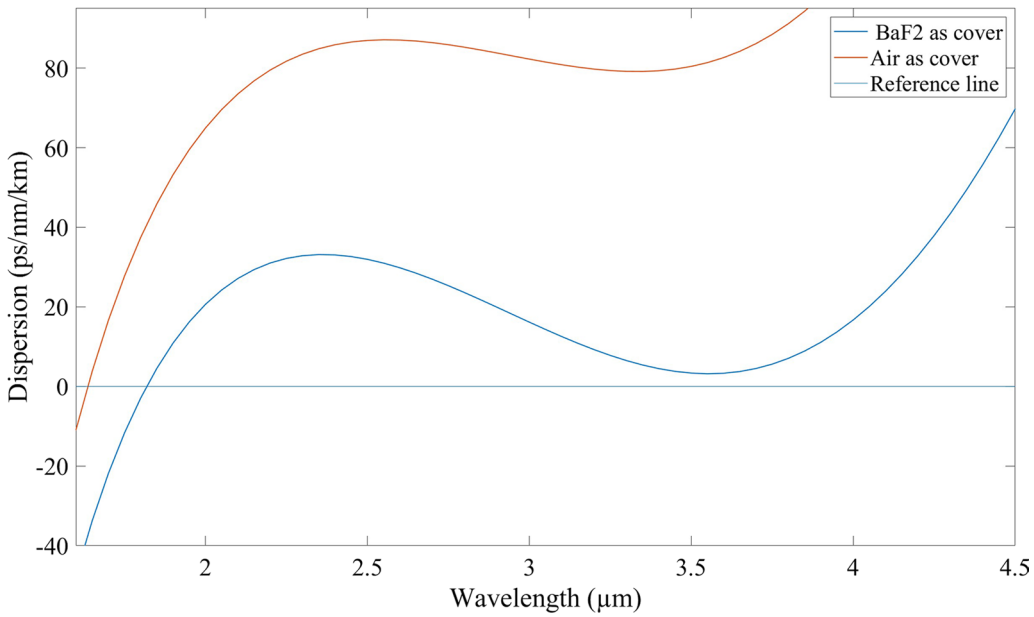

Fig. 7 Comparison between dispersion profiles of the SiN-coated TeO_2 hybrid waveguide with BaF_2 and air as cladding.

value, and the ZDW shifts towards a lower wavelength value, which was observed by numerical simulation.

Figure 6 shows the dispersion profile with optimized geometrical parameters of the hybrid waveguide, namely $h_1 = 470$ nm, $h_2 = 580$ nm, and $w = 3$ μm. With these optimized parameters, the dispersion curve varies from 40.60 ps/nm/km to 33.15 ps/nm/km within the spectral range of 1.55–4.25 μm, and the value of the ZDW is around 1.80 ps/nm/km. The dispersion curve lies in the anomalous domain upon optimized geometrical parameters. At pumping wavelengths 1.55 μm, 2 μm, 3 μm, and 4 μm observed dispersion values are −40.60 ps/nm/km, 20.64 ps/nm/km, 16.15 ps/nm/km, and 16.70 ps/nm/km, respectively. By using BaF_2 as covering, the low dispersion value varies from 3.192 ps/nm/km to 33.1368 ps/nm/km in the spectral range from 1.85 μm to 4.0 μm in comparison to no covering layer or air, as the covering layer dispersion varies from 89.1122 ps/nm/km to 79.18 ps/nm/km in the same spectral range. A low dispersion

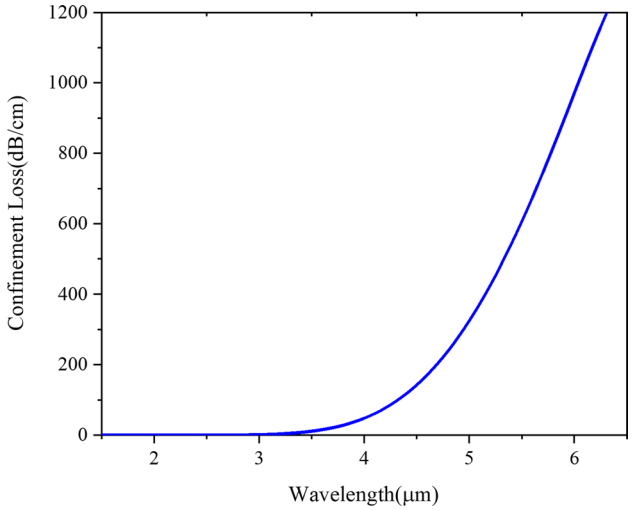

Fig. 8 Confinement loss of a SiN-coated TeO_2 hybrid waveguide with varied input laser pulse wavelengths.

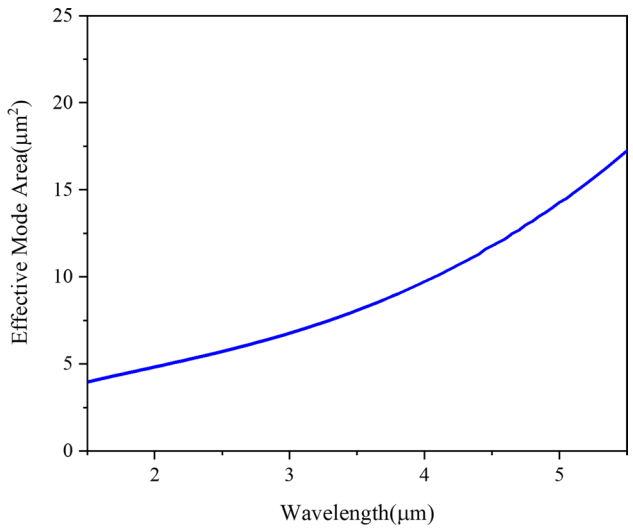

Fig. 9 Spectral variation in the effective mode area of an on-chip hybrid waveguide.

profile is crucial for maximizing SC spectral broadening. A comparison in dispersion characteristics of BaF_2 cover and air as cover is shown in the Fig. 7.

To benefit from TeO_2 material features such as high nonlinearity and light emission in rare-earth-doped films, large optical confinement inside the core is ideal. Figure 8 shows the modal confinement loss as a function of the wavelength of an input laser pulse. It can be seen that the value of confinement loss is in the range from 0.1×10^{-4} dB/cm to 35 dB/cm with spectral bandwidth of 1.5 to 4 μm. Confinement loss in a given hybrid waveguide structure increases sharply after 4.5 μm. Tellurite glasses are transparent in the spectral range

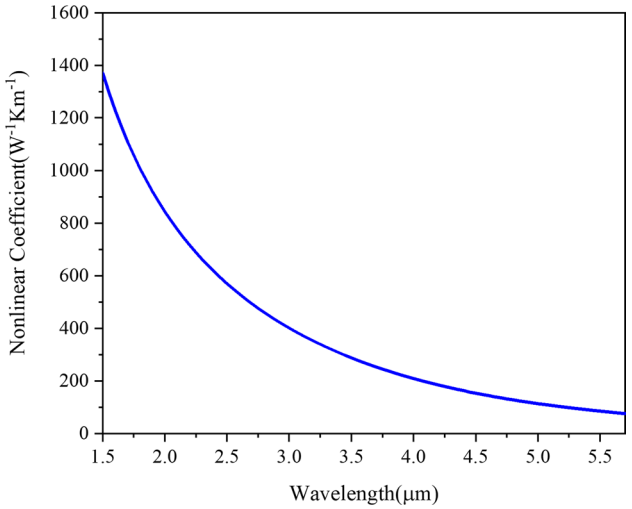

Fig. 10 Spectral variation in nonlinear coefficient of an on-chip hybrid waveguide.

below 5 μm. These materials exhibit significant material loss for longer wavelengths in the IR region. Saini et al., Feng et al., and Jha et al. independently studied the optical losses of tellurium oxide.[43,53,54] Their research shows large material and propagation loss beyond 5 μm in tellurite-based optical fibers, which sets the long-wavelength limit of mode confinement at 4.5 μm. This hybrid waveguide can be advantageous for nonlinear applications within the wavelength range up to 4.5 μm.

Spectral variations in the effective area of the fundamental TE mode which travels through this numerically simulated hybrid waveguide are presented in Fig. 9. It is noted that at pumping wavelengths of 1.55 μm, 1.80 μm, and 2 μm, the values of effective mode area are 4.06 μm^2, 4.5 μm^2, and 4.8 μm^2, respectively. For various nonlinear applications, the nonlinearity of the material must be high. The variation in the nonlinearity of a hybrid waveguide with the variation in the wavelength of the input laser pulse is presented in Fig. 10. It can be seen that the values of the nonlinear coefficient are 1297 W^{-1} km^{-1}, 1008 W^{-1} km^{-1}, and 843 W^{-1} km^{-1} at the pumping wavelengths 1.55 μm, 1.80 μm, and 2 μm, respectively.

Conclusion

We have designed and analyzed a SiN-coated TeO_2 on-chip hybrid waveguide for nonlinear applications. After the parameters of the hybrid waveguide are optimized, the dispersion characteristics are nearly flat and broad within the dispersion range of −40.60 ps/nm/km to 33.15 ps/nm/km for the spectral bandwidth of 1.50–4.25 μm, and the ZWD measures around 1.80 μm. To generate nonlinear effects in such types of on-chip waveguide devices, a commercially accessible fiber laser operating at 2.0 μm can

be employed. Pumping around the ZDW lowers the input power requirement and maximum transfer of energy to the output spectra. Results indicate that this design exhibits a low modal confinement loss for a wavelength range of 1.5–4 μm and very high nonlinear coefficient of 1297 $W^{-1}km^{-1}$ and 843 $W^{-1}km^{-1}$ at 1.55 μm and 2 μm operating wavelengths, respectively. The designed hybrid waveguide structure can be employed for future on-chip integrated devices. Results of numerical simulation confirm that this hybrid SiN-coated TeO_2 waveguide device can significantly aid in expanding its functionality for nonlinear optical applications across numerous domains, including on-chip light sources, frequency conversion, clinical investigations, four-wave mixing, Raman amplification, mid-IR imaging, and generation of mid-IR supercontinuum spectra, among many other domains.

Acknowledgments Kanika highly acknowledges the financial support under the Ph.D. fellowship scheme from director N.I.T. Kurukshetra. TSS and NJ highly acknowledge the financial support from the director N.I.T. Kurukshetra to carry out this research.

Conflict of nterest The authors declare no conflict of interest.

References

1. laud BB, Laser and Non-Linear Optics, 3rd Ed. (2011).
2. P. Govind, *Agrawal, nonlinear fiber optics*, 5th ed., (Oxford: Elsevier Academic Press, 2013).
3. H.K. Tsang, C.S. Wong, T.K. Liang, I.E. Day, S.W. Roberts, A. Harpin, J. Drake, and M. Asghari, Optical dispersion, two-photon absorption and self-phase modulation in silicon waveguides at 1.5 μm wavelength. *Appl. Phys. Lett.* 80, 416 (2002).
4. D. Dimitropoulos, R. Claps, Y. Han, and B. Jalali, *Nonlinear Optics in silicon waveguides: stimulated Raman scattering and two-photon absorption, integrated optics: devices, materials, and technologies VII*, Vol. 4987 (Bellingham: SPIE, 2003).
5. H. Fukuda, K. Yamada, T. Shoji, M. Takahashi, T. Tsuchizawa, T. Watanabe, J. Takahashi, S. Itabashi, D. Lee, H. Lim, A. Luan, J. Agarwal, and L. Foresi, Four-wave mixing in silicon wire waveguides. *Opt. Express* 13(12), 4629–4637 (2005).
6. J.M. Dudley and J.R. Taylor, *Supercontinuum generation in optical fibers* (Cambridge: Cambridge University Press, 2010).
7. T.S. Saini, A. Kumar, and R.K. Sinha, Design and modelling of dispersion-engineered rib waveguide for ultra-broadband mid-infrared supercontinuum generation. *J. Mod. Opt.* 64, 143–149 (2017).
8. T.S. Saini, A. Baili, V. Dahiya, A. Kumar, R. Cherif, M. Zghal, and R.K. Sinha, *Design of equiangular spiral photonic crystal fiber for supercontinuum generation at 1550 nm, in photonic fiber and crystal devices: advances in materials and innovations in device applications VIII*, Vol. 9200 (Bellingham: SPIE, 2014), p.920012.
9. T.S. Saini and R.K. Sinha, Mid-infrared supercontinuum generation in soft-glass specialty optical fibers: a review. *Progr. Quantum Electron* 78, 100342 (2021).
10. D.R. Solli, C. Ropers, and B. Jalali, Active control of rogue waves for stimulated supercontinuum generation. *Phys. Rev. Lett.* (2008). https://doi.org/10.1103/PhysRevLett.101.233902.
11. C. Dunsby, P.M.P. Lanigan, J. McGinty, D.S. Elson, J. Requejo-Isidro, I. Munro, N. Galletly, F. McCann, B. Treanor, B. Onfelt, D.M. Davis, M.A.A. Neil, and P.M.W. French, An electronically tunable ultrafast laser source applied to fluorescence imaging and fluorescence lifetime imaging microscopy. *J. Phys. D Appl. Phys.* 37, 3296 (2004).
12. A. Schliesser, N. Picqué, and T.W. Hänsch, Mid-infrared frequency combs. *Nat. Photonics* 6, 440–449 (2012).
13. P.L. Hsiung, Y. Chen, T.H. Ko, J.G. Fujimoto, C.J. de Matos, S.V. Popov, and V.P. Gapontsev, Optical coherence tomography using a continuous-wave, high-power Raman continuum light source. *Opt. Express* 12(22), 5287–5295 (2004).
14. S.T. Sanders, Wavelength-agile fiber laser using group-velocity dispersion of pulsed super-continua and application to broadband absorption spectroscopy. *Appl. Phys. B* 75, 799 (2002).
15. J.K. Ranka, R.S. Windeler, and A.J. Stentz, Visible continuum generation in air-silica microstructure optical fibers with anomalous dispersion at 800 Nm. *Opt. Lett.* 25(1), 25–27 (2000).
16. M. Liao, C. Chaudhari, G. Qin, X. Yan, T. Suzuki, and Y. Ohishi, Tellurite microstructure fibers with small hexagonal core for supercontinuum generation. *Opt. Express* 17(14), 12174–21218 (2009).
17. W. Yuan, 2–10 Mm mid-infrared supercontinuum generation in as2se 3 photonic crystal fiber. *Laser Phys. Lett.* 10, 0951107 (2013).
18. L. Liu, G. Qin, Q. Tian, D. Zhao, and W. Qin, Numerical investigation of mid-infrared supercontinuum generation up to 5 Mm in single mode fluoride fiber. *Opt. Express* 19(11), 10041–10048 (2011).
19. T.S. Saini, A. Kumar, and R.K. Sinha, Design and analysis of dispersion engineered rib waveguides for on-chip mid-infrared supercontinuum. *J. Lightwave Technol.* 36, 1993–1999 (2018).
20. Saini TS, Kumar A, Sinha RK, Highly Nonlinear Triangular Core Photonic Crystal Fiber with All Normal Dispersion for Supercontinuum Generation. In Frontiers in Optics (pp. FW1D-4), Optica Publishing Group (2014).
21. N. Nader, A. Kowligy, J. Chiles, E.J. Stanton, H. Timmers, A.J. Lind, and R.P. Mirin, Infrared frequency comb generation and spectroscopy with suspended silicon nanophotonic waveguides. *Optica* 6, 1269–1276 (2019).
22. N. Zhang, X. Peng, Y. Wang, S. Dai, Y. Yuan, J. Su, G. Li, P. Zhang, P. Yang, and X. Wang, Ultrabroadband and coherent mid-infrared supercontinuum generation in Te-based chalcogenide tapered fiber with all-normal dispersion. *Opt. Express* 27, 10311 (2019).
23. T.S. Saini, T.H. Tuan, T. Suzuki, and Y. Ohishi, Coherent mid-IR supercontinuum generation using tapered chalcogenide step-index optical fiber: experiment and modelling. *Sci. Rep.* 10(1), 2236 (2020).
24. Z. Eslami, L. Salmela, A. Filipkowski, D. Pysz, M. Klimczak, R. Buczynski, J.M. Dudley, and G. Genty, Two octave supercontinuum generation in a non-silica graded-index multimode fiber. *Nat. Commun.* 13(1), 2126 (2022).
25. Y. Zheng, C. Sun, B. Xiong, L. Wang, Z. Hao, J. Wang, and Y. Luo, Integrated gallium nitride nonlinear photonics. *Laser Photonics Rev.* 16(1), 2100071 (2022).
26. A. Khamaru, K. Sharma, D.S. Tomer, and A. Kumar, Mid-IR supercontinuum generation in dispersion flattened As38Se62chalcogenide photonic crystal Fiber. *J. Phys. Conf. Ser.* 2426, 012002 (2023).
27. K. Xia, Z. Yang, P. Zhao, P. Yang, P. Xu, L. Xu, X. Peng, W. Zhang, S. Dai, S. Wang, and Q. Nai, Supercontinuum generation in As_2S_3 chalcogenide waveguide pumped by all-fiber structured dual-femtosecond solitons. *Opt. Express* 31, 29440 (2023).
28. J.W. Choi, Z. Han, B.U. Sohn, G.F.R. Chen, C. Smith, L.C. Kimerling, K.A. Richardson, A.M. Agarwal, and D.T.H. Tan,

Nonlinear characterization of GeSbS chalcogenide glass waveguides. *Sci. Rep.* 6, 39234 (2016).
29. T.S. Saini, U.K. Tiwari, and R.K. Sinha, Rib waveguide in Ga-Sb-S chalcogenide glass for on-chip mid-IR supercontinuum sources: design and analysis, *J Appl Phys.* 122 (2017).
30. T.S. Saini, N.P. Trung Hoa, K. Nagasaka, X. Luo, T.H. Tuan, T. Suzuki, and Y. Ohishi, Coherent midinfrared supercontinuum generation using a rib waveguide pumped with 200 Fs laser pulses at 28 Mm. *Appl. Opt.* 57, 1689 (2018).
31. A. Medjouri, D. Abed, O. Ziane, and L.M. Simohamed, Design and optimization of As2S5 chalcogenide channel waveguide for coherent mid-infrared supercontinuum generation. *Optik* 154, 811 (2018).
32. M. Sinobad, A.D. Torre, R. Armand, B. Luther-Davies, P. Ma, S. Madden, A. Mitchell, D.J. Moss, J.M. Hartmann, J.M. Fédéli, C. Monat, and C. Grille, High coherence at f and 2f of mid-infrared supercontinuum generation in silicon germanium waveguides. *IEEE J. Sel. Top. Quantum Electron.* 26, 18 (2019).
33. A.D. Torre, M. Sinobad, R. Armand, B. Luther-Davies, P. Ma, S. Madden, A. Mitchell, D.J. Moss, J.M. Hartmann, V. Reboud, J.M. Fedeli, C. Monat, and C. Grillet, Mid-infrared supercontinuum generation in a low-loss germanium-on-silicon waveguide. *APL Photonics*. 6 (2021).
34. F. Gyger, J. Liu, F. Yang, J. He, A.S. Raja, R.N. Wang, S.A. Bhave, T.J. Kippenberg, and L. Thévenaz, Observation of stimulated brillouin scattering in silicon nitride integrated waveguides. *Phys. Rev. Lett.* 124(1), 013902 (2020).
35. T.S. Saini and V.R. Supradeepa, Tellurium-oxide coated silicon-nitride hybrid waveguide for near-to-mid-IR supercontinuum generation: design and analysis. *J. Mod. Opt.* 68, 29 (2021).
36. J. Zhang, S. Zhang, X. Jiang, J. Yao, A. Wang, and Q. Zhan, Numerical study on flat dispersion in a single-layer Si3N4 coupled-waveguides with four zero-dispersion wavelengths for supercontinuum generation. *Opt. Laser Technol.* 160, 109061 (2023).
37. M. Sheikhmolaee, M.R. Alizadeh, S. Olyaee, and M. Seifouri, Supercontinuum generation in tapered planar rib waveguide based on gap-se hybrid chalcogenide. *Opt Quantum Electron* 56(1), 4 (2023).
38. Botter R, Segat Frare B, Hashemi B, Ye K, Klaver Y, Bradley J, and Marpaung D, Observation and enhancement of stimulated brillouin scattering in tellurite covered silicon nitride waveguides, arXiv preprint arXiv:2307.12814 (2023).
39. Mbonde HM, Singh N, Segat Frare BL, Sinobad M, Torab Ahmadi P, Hashemi B, Bonneville DB, Mascher P, Kärtner FX, and Bradley JDB, octave-spanning supercontinuum generation in a CMOS-compatible thin Si_3N_4 waveguide coated with highly nonlinear TeO_2. arXiv preprint arXiv:2309.08318 (2023).
40. V.A.G Rivera and D. Manzani, *Technological advances in tellurite glasses properties, processing, and applications* (New York: Springer, 2017)
41. K. Vu, S. Farahani, and S. Madden, 980nm pumped erbium doped tellurium oxide planar rib waveguide laser and amplifier with gain in S C and L Band. *Opt. Express* 23, 747 (2015).
42. R. Amin, L.F. Abdulrazak, S.R. Tahhan, N. Mohammadd, K. Ahmed, F.M. Bui, and S.M. Ibrahim, Tellurite glass based optical fiber for the investigation of supercontinuum generation and nonlinear properties. *Phys. Scr.* 97, 030007 (2022).
43. T.S. Saini, S. Arora, and V.R. Supradeepa, Far-detuned mid-IR wavelength conversion at 4.05 μm in a tellurium oxide rib waveguide pumped at 1550 Nm: design and analysis, *AIP Adv*. 11 (2021).
44. H.C. Frankis, K.M. Kiani, D.B. Bonneville, C. Zhang, S. Norris, R. Mateman, A. Leinse, N.D. Bassim, A.P. Knights, and J.D.B. Bradley, Low-loss TeO 2 -coated Si 3 N 4 waveguides for application in photonic integrated circuits. *Opt. Express* 27, 12529 (2019).
45. S.J. Madden, K.T. Vu, D.A. Gaponov, and A.S. Biryukov, Very low loss reactively ion etched tellurium dioxide planar rib waveguides for linear and non-linear optics. *Opt. Express* 17(20), 17645–17651 (2009).
46. S. Romero-García, F. Merget, F. Zhong, H. Finkelstein, and J. Witzens, Silicon nitride CMOS-compatible platform for integrated photonics applications at visible wavelengths. *Opt. Express* 21, 14036 (2013).
47. P. Muñoz, G. Micó, L.A. Bru, D. Pastor, D. Pérez, J.D. Doménech, J. Fernández, R. Baños, B. Gargallo, R. Alemany, A.M. Sánchez, J.M. Cirera, R. Mas, and C. Domínguez, Silicon nitride photonic integration platforms for visible, near-infrared and mid-infrared applications. *Sensors* 17, 2088 (2017).
48. K. Wörhoff, R.G. Heideman, A. Leinse, and M. Hoekman, TriPleX: a versatile dielectric photonic platform. *Adv. Opt. Technol* 4(2), 189–207 (2015).
49. C.G.H. Roeloffzen et al., Low-loss Si3n4 triplex optical waveguides: technology and applications overview. *IEEE J. Sel. Top. Q Electron* 24(4), 1–21 (2018).
50. E.D. Palik, *Handbook of optical constants of solids* (Cambridge: Academic Press, 1998).
51. Z.S. Matar, M. Al-Dossari, S.K. Awasthi, N.S. Abd El-Gawaad, H. Hanafy, R.M. Amin, M.I. Fathy, and A.H. Aly, Theoretical study on polycarbonate-based one-dimensional ternary photonic structures from far-ultraviolet to near-infrared regions of electromagnetic spectrum. *Crystals (Basel)* 12, 642 (2022).
52. Astruc B, Marianne, Boivin D, and Sillard P, Design and fabrication of weakly-coupled few-modes fibers, IEEE photonics society summer topicals Seattle, Washington, (2012).
53. X. Feng, A.K. Mairaj, D.W. Hewak, and T.M. Monro, Nonsilica glasses for holey fibers. *J. Lightwave Technol.* 23(6), 2046–2054 (2005). https://doi.org/10.1109/JLT.2005.849945.
54. A. Jha, B.D.O. Richards, G. Jose, T.T. Fernandez, C.J. Hill, J. Lousteau, and P. Joshi, Review on structural, thermal, optical and spectroscopic properties of tellurium oxide based glasses for fibre optic and waveguide applications. *Int. Mat. Rev.* 57(6), 357–382 (2012).